J Paleolimnol (2013) 50:207–229
DOI 10.1007/s10933-013-9715-9

ORIGINAL PAPER

Diatom–environment relationships and a transfer function for conductivity in lakes of the Badain Jaran Desert, Inner Mongolia, China

Patrick Rioual · Yanbin Lu · Handong Yang · Louis Scuderi · Guoqiang Chu · Jonathan Holmes · Bingqi Zhu · Xiaoping Yang

Received: 24 January 2012 / Accepted: 5 April 2013 / Published online: 17 April 2013

Abstract We describe a dataset of 26 modern diatom samples and associated environmental variables from the Badain Jaran Desert, northwest China. The influence of electrical conductivity (EC) and other variables on diatom distribution was explored using multivariate analyses and generalized additive modeling of species response curves. A transfer function was derived for EC, the variable with the largest unique effect on diatom variance, as shown by partial canonical correspondence analysis. Weighted-averaging partial least squares regression and calibration provided the best model, with a high coefficient of determination ($r^2_{boot} = 0.91$) and low prediction error ($RMSEP_{boot} = 0.136 \log_{10} \mu S\ cm^{-1}$). To assess its potential for palaeosalinity and palaeoclimate reconstructions, the EC transfer function was applied to fossil diatom assemblages from ^{210}Pb-dated short sediment cores collected from two subsaline lakes of the Badain Jaran Desert. The diatom-inferred (DI) EC reconstructions were compared with meteorological data for the past 50 years and with remote sensing data for the period AD 1990–2012. Changes in DI–EC were small and their relationship with climate was weak. Moreover, remote sensing data indicate that the surface areas and water depths of these lakes did not change, which suggests that water loss by evaporation is compensated

Electronic supplementary material The online version of this article (doi:10.1007/s10933-013-9715-9) contains supplementary material, which is available to authorized users.

P. Rioual (✉) · Y. Lu · G. Chu · X. Yang
Key Laboratory of Cenozoic Geology and Environment, Institute of Geology and Geophysics, Chinese Academy of Sciences, Beijing 100029, China
e-mail: prioual@mail.igcas.ac.cn

Y. Lu
e-mail: luyb03@gmail.com

G. Chu
e-mail: chuguoqiang@mail.igcas.ac.cn

X. Yang
e-mail: xpyang@mail.igcas.ac.cn

H. Yang · J. Holmes
Environmental Change Research Centre, University College London, Pearson Building, Gower Street, London WC1E 6BT, UK
e-mail: handong.yang@ucl.ac.uk

J. Holmes
e-mail: j.holmes@ucl.ac.uk

L. Scuderi
Department of Earth and Planetary Sciences, University of New Mexico, MSC03 2040, Albuquerque, NM 87131, USA
e-mail: tree@unm.edu

B. Zhu
Key Laboratory of Water Cycle and Related Land Surface Processes, Institute of Geographic Sciences and Natural Resources Research, Chinese Academy of Sciences, Beijing 100101, China
e-mail: zhubingqi@igsnrr.ac.cn

by groundwater inflow. These results suggest that the response of these lakes to climate change is mediated by non-climatic factors such as the hydrogeological setting, which control recharge from groundwater, and may be non-linear and non-stationary.

Keywords Diatoms · Transfer function · Electrical conductivity · Saline lakes · Badain Jaran Desert · China

Introduction

The Badain Jaran Desert, in western Inner Mongolia (China) is characterized by a unique landscape in which megadunes, the tallest in the world, coexist with >100 permanent spring-fed lakes (Yang 2000). In recent years, research in this desert has focused mainly on the geomorphology and evolution of the megadunes (Yang XP et al. 2003), the source of recharge for the inter-dune lakes, past lake-level fluctuations recorded in former shorelines (Yang et al. 2010) and the geochemistry of the lakes and groundwater (Yang and Williams 2003). There is, however, scant knowledge on the current limnology of these lakes and no palaeolimnological work has been published. It is known, however, that lakes in the Badain Jaran Desert show a wide range in salinity, from subsaline to hypersaline (Hofmann 1996; Yang and Williams 2003).

Closed-basin lakes in arid regions respond rapidly to climate-driven changes in hydrology, with oscillations in the balance between precipitation and evaporation having an impact on both changes in lake level and the concentration of dissolved salts (Fritz 2008). The situation is more complicated for lakes in the Badain Jaran Desert. Although there are neither streams discharging into them nor outlets draining them, these lakes cannot be considered strictly closed-basin lakes as they are fed by freshwater springs and can be considered seepage lakes (Hofmann 1996). Nevertheless, recent work has shown that local precipitation makes a significant contribution to groundwater recharge of these lakes and that their past water-level variations should reflect palaeoclimatic changes (Yang et al. 2010).

Among the environmental indicators that can be found in lake sediments from arid regions, diatoms, which are unicellular algae with a cell wall composed of silica (Si), have been widely used to reconstruct past changes in limnological variables, in particular lake-water salinity and related variables such as electrical conductivity (EC) and concentrations of anions and cations (Fritz et al. 1993; Gasse et al. 1995; Wilson et al. 1996; Gell 1997; Reed 1998; Davies et al. 2002; Ryves et al. 2002; Verleyen et al. 2003; Yang XD et al. 2003; Shinneman et al. 2009; Wang et al. 2011; Reed et al. 2012).

Our research on the lakes of the Badain Jaran had two aims. First, we explored the relationship between the composition of diatom assemblages in surface sediment samples and lake-water chemistry and developed diatom-based transfer-functions. Second, we applied one of these transfer functions to diatom records from short sediment cores to infer recent changes in lake conditions. This work contributes to the wider application of lacustrine diatoms for the study of Holocene climate variability in the drylands of northern China and Central Asia.

Study area

We focused on the southeastern Badain Jaran Desert, from 102°14 to 102°31′E and 39°33 to 39°53′N, where most lakes are located (Fig. 1). The lakes have a narrow range of altitude, 1,162–1,337 m above sea level. Surface morphology consists of sand dunes with a maximum height of 460 m. The regional climate is strongly continental and hyper-arid. During the winter months, this desert is under the influence of the dry and cold air masses associated with the high-pressure system centered over Mongolia. At the weather station of Ekenhuduge town, in Alashan Youqi county, at the southern edge of the desert (39°12′N, 101°40′E), the mean annual temperature is 7.7 °C, and mean monthly temperature ranges from −10 °C in January to +25 °C in July. The average annual precipitation is 118 mm, but inter-annual variation is very high. More than half of the precipitation falls in the summer months between June and August, and is derived from the East Asian summer monsoon. Diurnal temperatures in summer months range from 0 to >40 °C (Yang and Williams 2003; Yang XP et al. 2003).

Materials and methods

Physical and chemical variables

Forty-two lakes were sampled during four field campaigns in June 2007, October 2008, March and

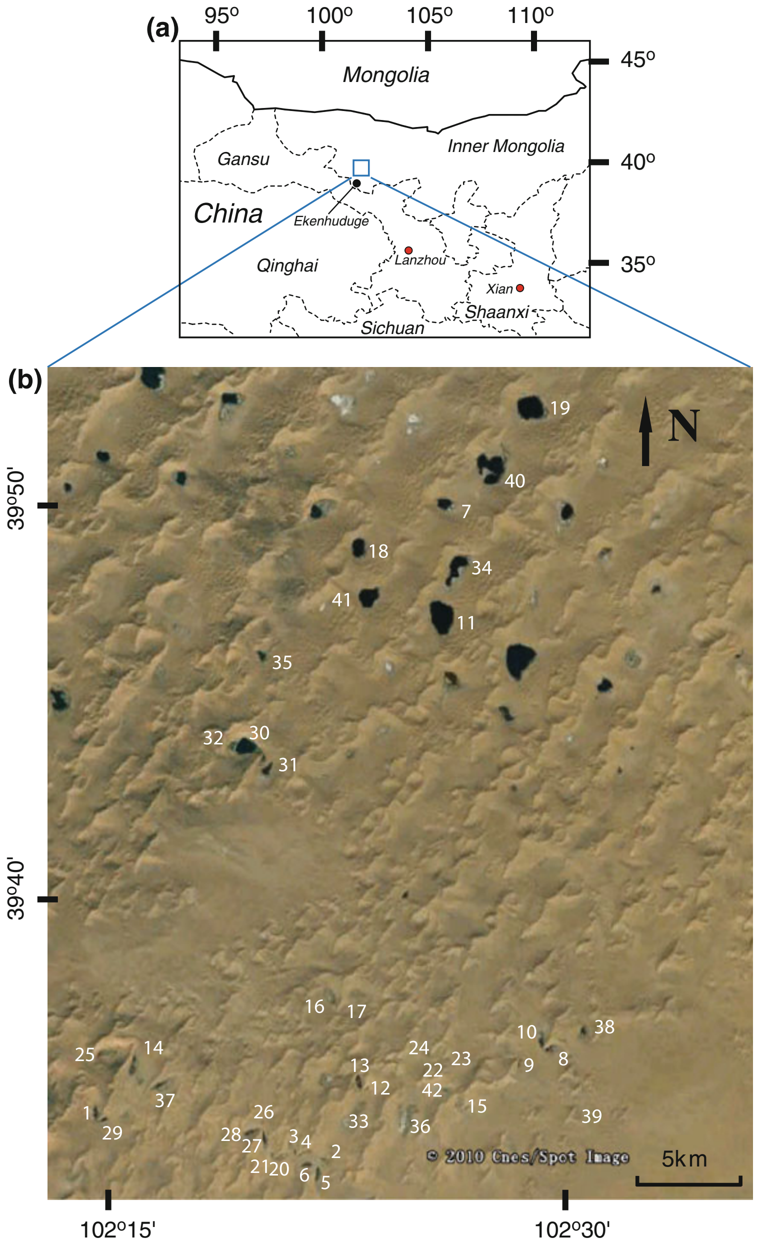

Fig. 1 *Map* of the study area in north-central China (**a**) and sampled sites in the Badain Jaran desert (**b**). In **a**, the location of the nearest meteorological station (Ekenhuduge town, Alashan Youqi county) is given. **b** Satellite image of the south-east corner of the BadainJaran Desert, showing the 42 lakes sampled in this study. Lakes included in the current research are *labeled* according to their *number* in Table 1

October 2009 (Fig. 1; Table 1). Altitude, latitude and longitude of sampling sites were measured in the field using a Magellan® handheld GPS. Lake area was estimated from topographic maps and satellite images (Google Earth Pro®). For water chemistry analysis, surface water samples were collected by hand (~0.3 m depth) from the deepest part of each lake, as determined either with a hand-held acoustic depth meter in deep lakes or with a ruler for shallow lakes. Some lakes were sampled up to three times from 2007 to 2009, although most were sampled once.

EC, pH, total alkalinity (Alk), total phosphorus (TP) and total nitrogen (TN) were measured on unfiltered lake water. Anions (Cl^-, SO_4^{2-}, NO_3^-), cations (Ca^{2+}, Mg^{2+}, K^+, Na^+), dissolved organic carbon (DOC) and dissolved Si were measured on water filtered through Whatman GF/F® glass fiber filters. Anion concentrations were measured on a

Table 1 Geographical location, maximum depth, lake area, electrical conductivity and salinity of the 42 lakes included in the Badain Jaran dataset (the date of sampling is indicated in the last column on the right)

S. no.	Lake name	Code	Latitude (°)	Longitude (°)	Altitude (m asl)	Depth (m)	Area (ha)	EC 25 (mS/cm)	Salinity (g/L)	Date
1	Aer Jilin	AERJ	39.34.319N	102.14.485E	1,202	1.70	7.3	2.4	2.0	Jun-07
2	*Badan Bei Hu 1*	*BADB1*	*39.33.720N*	*102.21.078E*	*1,212*	*0.20*	*0.3*	*131.1*	*160.0*	*Oct-08*
3	Badan Bei Hu 2	BADB2	39.33.399N	102.21.180E	1,208	0.90	1.0	11.6	9.8	Oct-08
4	Badan Bei Hu 3	BADB3	39.33.387N	102.21.312E	1,208	0.50	0.3	38.1	30.3	Oct-08
5	Badan Dong Hu	BADD	39.33.120N	102.21.859E	1,202	1.40	6.5	2.5	1.6	Oct-08
6	*Badan Xi Hu*	*BADX*	*39.33.157N*	*102.21.733E*	*1,201*	*N/a*	*7.1*	*152.8*	*178.7*	*Oct-08*
7	*Baga Jilin*	*BAGA*	*39.50.080N*	*102.25.205E*	*1,178*	*4.20*	*23.8*	*211.0*	*175.8*	*Oct-08*
8	Baoritelegai Dong Hu	BAOD	39.36.391N	102.29.295E	1,280	2.50	5.2	2.5	1.5	Oct-08
9	Baoritelegai Nan Hu	BAON	39.36.030N	102.28.434E	1,274	0.50	1.9	2.2	1.4	Oct-08
10	Baoritelegai Xi Hu	BAOX	39.36.452N	102.29.199E	1,276	1.60	10.8	2.8	1.8	Oct-08
11	*Barun Jilin*	*BARU*	*39.47.731N*	*102.25.050E*	*1,179*	*7.50*	*128.3*	*130.2*	*84.5*	*Oct-08*
12	Dugui Jilin Dong Hu	DUGD	39.35.167N	102.23.430E	1,198	0.50	1.3	3.3	2.3	Oct-08
13	Dugui Jilin Xi Hu	DUGX	39.35.252N	102.23.174E	1,205	0.30	0.5	3.5	5.4	Oct-08
14	Dunde Jilin	DUND	39.35.714N	102.15.729E	1,203	1.00	5.1	6.0	4.9	Jun-07
15	Haisen Jilin	HAIS	39.34.842N	102.26.409E	1,212	0.50	0.2	5.7	3.9	Oct-08
16	Halareritu	HALA	39.37.353N	102.22.200E	1,191	1.05	1.6	2.0	1.3	Oct-09
17	Halareritu Dong Hu	HALD	39.37.182N	102.22.508E	1,188	0.30	0.1	4.8	3.4	Oct-09
18	*Huduge Jilin*	*HUDU*	*39.48.799N*	*102.22.511E*	*1,174*	*5.50*	*43.3*	*206.6*	*115.2*	*Oct-08*
19	*Huhe Jilin*	*HUHE*	*39.52.468N*	*102.27.650E*	*1,188*	*10.70*	*103.0*	*19.7*	*16.6*	*Oct-08*
20	*Huhewuzhu'er Dong Hu*	*HHWD*	*39.33.387N*	*102.20.854E*	*1,204*	*0.20*	*0.2*	*150.8*	*111.0*	*Oct-08*
21	Huhewuzhu'er Xi Hu	HHWX	39.33.398N	102.20.397E	1,202	1.20	0.5	117.0	95.3	Oct-08
22	Hulusitai Dong Hu 1	HULD1	39.36.092N	102.25.484E	1,209	0.20	0.2	2.4	2.4	Oct-08
23	Hulusitai Dong Hu 2	HULD2	39.36.032N	102.26.037E	1,216	0.75	0.2	1.9	1.1	Oct-08
24	Hulusitai Xi Hu	HULX	39.36.124N	102.25.435E	1,209	1.50	0.5	6.1	4.0	Oct-08
25	Mudan Jilin	MUDA	39.35.744N	102.14.591E	1,199	0.80	3.5	1.4	1.3	Oct-09
26	*Sayinwusu Bei Hu*	*SAYB*	*39.34.185N*	*102.20.038E*	*1,203*	*0.55*	*0.2*	*63.5*	*83.7*	*Oct-08*
27	Sayinwusu Dong Hu	SAYD	39.33.804N	102.20.176E	1,213	1.30	7.0	29.2	25.0	Oct-08
28	Sayinwusu Xi Hu	SAYX	39.34.014N	102.19.867E	1,204	1.20	9.3	21.5	20.3	Oct-08
29	Shao Bai Jilin	SHAO	39.34.037N	102.14.778E	1,204	1.40	5.1	2.5	2.0	Jun-07
30	*Shuang Haizi*	*SHHA*	*39.43.848N*	*102.19.216E*	*1,178*	*9.70*	*51.2*	*123.1*	*173.6*	*Jun-07*
31	*Shuang Haizi Dong Hu*	*SHHD*	*39.43.164N*	*102.19.529E*	*1,186*	*6.40*	*13.8*	*137.9*	*180.2*	*Jun-07*
32	Shuang Haizi Xi Hu	SHHX	39.43.674N	102.18.463E	1,162	0.50	0.5	9.2	6.9	Oct-09
33	*Suhaitu*	*SUHA*	*39.34.173N*	*102.22.902E*	*1,203*	*0.10*	*1.0*	*215.2*	*228.6*	*Oct-08*
34	*Sumu Jilin*	*SUMU*	*39.48.099E*	*102.25.354E*	*1,182*	*2.50*	*62.5*	*137.2*	*112.7*	*Oct-08*
35	*Tamaying*	*TAMA*	*39.45.950N*	*102.19.366E*	*1,169*	*2.70*	*10.7*	*175.7*	*136.9*	*Oct-08*
36	*Tonggutu*	*TONG*	*39.34.236N*	*102.24.733E*	*1,212*	*0.10*	*0.2*	*494.7*	*236.9*	*Oct-08*
37	Women Jilin	WOME	39.34.974N	102.16.569E	1,206	0.60	4.6	2.9	2.1	Jun-07
38	Wosigetu Nuoer	WOSI	39.36.872N	102.30.486E	1,286	1.30	9.9	1.7	1.3	Oct-08
39	Xiao Haizi	XIAH	39.33.515N	102.29.217E	1,337	0.40	0.1	3.1	2.1	Oct-08
40	*Yinde'ertu*	*YIND*	*39.51.179N*	*102.26.388E*	*1,168*	*8.00*	*114.9*	*189.5*	*179.4*	*Oct-08*
41	*Zhalate*	*ZHAL*	*39.47.451N*	*102.22.690E*	*1,180*	*6.90*	*62.6*	*141.6*	*110.2*	*Oct-08*
42	Zhunaogeqi	ZHUN	39.35.255N	102.26.033E	1,209	1.10	3.9	2.5	1.8	Oct-09

Values in italics are lakes for which no diatoms were found in surface sediment

Dionex ICS 1500 ion chromatograph and cations on an ICP–MS at IGG–CAS. Alk was measured by Gran titration (Gran 1952). From the Gran titration results, concentrations of CO_3^{2-} and HCO_3^- were computed using an online calculator (http://or.water.usgs.gov/alk/methods.html). DOC was measured on a Shimadzu Total Organic Carbon analyzer at Tsinghua University, Beijing. TP analysis was done using an acid persulfate digestion and spectrophotometry, following the method developed by the Arctic Long Term Ecological Research (ARC-LTER) team (http://ecosystems.mbl.edu/arc/streams/protocol2.html). For TN analysis, persulfate oxidation was followed by nitrate analysis with spongy cadmium (Jones 1984; Bronk et al. 2000). Si was measured by colorimetry (Wetzel and Likens 2000).

Environmental dataset

For lakes in which several water samples were collected ($n = 5$), we found that water chemistry varied according to the month of the year when samples were collected. EC values, in particular, were higher in October than in March or June. To minimize the potential effect of these seasonal differences on the dataset, we chose values from October when available ($n = 36$), except for six lakes for which there were only values from June 2007 (Table 1). EC values were standardized to 25 °C (Endoh et al. 2008). Because solute composition and absolute concentration of major ions may be important determinants of diatom distribution, major ions were expressed both as equivalent concentrations (μ eq L^{-1}) and as molar proportions (%) of cation and anion sums. Two ionic ratios were also calculated, the cation ratio [ratio of alkali: alkaline earth metals, $(Na^+ + K^+)/(Mg^{2+} + Ca^{2+})$], and the anion ratio [Alk: major anions, $Alk/(Cl^- + SO_4^{2-})$] (Gasse et al. 1995). Salinity, expressed in g L^{-1}, was calculated by summing the concentrations of all the major cations and anions (Ca^{2+}, Mg^{2+}, K^+, Na^+, SO_4^{2-}, Cl^-, HCO_3^-, CO_3^{2-}). Altogether, 26 explanatory variables were explored (Table 2).

Surface-sediment sample collection and diatom analysis

Using an Uwitec® gravity corer, surface-sediment samples (the uppermost 1 cm) were taken from the deepest point of each lake. In addition to the surface sediment, we also analyzed samples from the littoral zone (epipsammon and epiphyton if macrophytes and/or *Phragmites* were present). Only surface sediment samples were included in the calibration dataset as these are considered to be sub-fossil and most analogous to sediment core assemblages. Sediment samples were prepared using the water-bath method (Renberg 1990). Diatom concentration was estimated using the microsphere method of Battarbee and Kneen (1982) and expressed as number of valves per gram dry matter (valves g dm^{-1}). Sub-samples of the cleaned, homogenized suspensions were diluted with distilled water and left to settle onto round glass coverslips and dry overnight in ambient conditions. Coverslips were mounted on glass slides with Naphrax®. Counting was done with a Leica DM LB2 microscope using bright-field and phase-contrast oil immersion optics at 1,000× magnification. For surface sediments, at least 500 diatom valves were enumerated, except in one sample, Haisen Jilin, which was characterized by severe diatom dissolution. At least 300 valves were counted for down-core samples. Diatom dissolution in surface samples and down-core samples was estimated following the method of Ryves et al. (2006), in which the fraction of valves without visible signs of dissolution is expressed as a proportion of all valves counted. This ratio, the F-index, varies from 0 (all valves partly dissolved) to 1 (perfect preservation). General and regional diatom floras (Cumming et al. 1995; Witkowski et al. 2000; Metzeltin et al. 2009; Hofmann et al. 2011) as well as genera-specific references (Krammer 1997; Lange-Bertalot 2001; Levkov 2009) were consulted for identification. Digital photographs of all identified taxa were taken during counting to aid taxonomic consistency.

Numerical methods

Multivariate ordinations were used to explore the relationships among lakes and species assemblages, and to establish whether differences in diatom assemblages were strongly associated with the main measured environmental gradients. Prior to the analyses, explanatory variables with skewed distributions were transformed to reduce the influence of extreme values. Three types of transformation, square-root, $\log_{10}$, $\log_{10}(x + 1)$, were tested for their ability to normalize the measured variables (Table 2).

Table 2 Summary of the 26 environmental variables measured from the 26 lakes in the diatom surface-sediment training set, with units, summary statistics, transformation applied in numerical analyses and results of constrained CCA on square-root transformed species data, using one single environmental variable at a time (marginal effect)

Variables	Code	Unit	Average	Max	Min	Median	Transformation	Constrained CCA λ_1	λ_1/λ_2	Marginal variance (%)
pH	pH		8.76	10.40	7.75	9.46	None	0.11	0.23	4.7
Electrical Conductivity	EC	$\mu S\ cm^{-1}$	7,355	38,149	1,371	2,978	Log(x)	0.41	1.30	18.0**
Total Phosphorus	TP	$\mu g\ L^{-1}$	33	187	0	23	Square root	0.24	0.57	10.4**
Total Nitrogen	TN	$\mu g\ L^{-1}$	4,195	12,676	956	3,026	Log(x)	0.33	1.03	14.5**
Nitrate-nitrogen	NO3	μ eq L^{-1}	594	3,628	0	175	Log(x + 1)	0.14	0.34	6.3*
Dissolved organic carbon	DOC	$mg\ L^{-1}$	32.8	143.1	4.9	11.2	Log(x)	0.35	1.05	15.4**
Dissolved silica	Si	$mg\ L^{-1}$	2.8	10.8	0.0	1.5	Log(x + 1)	0.08	0.17	3.5
Salinity	Salinity	$g\ L^{-1}$	6.0	30.3	1.1	2.2	Log(x)	0.40	1.25	17.3**
Total alkalinity	Alk	μ eq L^{-1}	26,729	95,935	2,340	10,670	Log(x)	0.32	0.96	13.9**
Chloride	Cl	μ eq L^{-1}	52,134	315,754	5,611	17,919	Log(x)	0.41	1.28	17.7**
Sulphate	SO4	μ eq L^{-1}	29,523	171,008	4,427	10,088	Log(x)	0.39	1.20	16.9**
% Alkalinity	%Alk	% anions	26.3	63.0	11.0	25.6	None	0.12	0.26	5.3
% Chloride	%Cl	% anions	46.2	61.0	20.2	45.8	None	0.09	0.19	3.8
% Sulphate	%SO4	% anions	27.0	39.7	11.5	29.0	None	0.13	0.27	5.6
Anion ratio	Anion-R	Alk: ($Cl + SO_4$)	0.41	1.73	0.12	0.34	Square root	0.12	0.25	5.1
Calcium	Ca	μ eq L^{-1}	1,242	3,653	310	1,041	Square root	0.14	0.30	6.1*
Potassium	K	μ eq L^{-1}	2,200	11,950	248	724	Log(x)	0.37	1.17	16.4**
Magnesium	Mg	$\mu eq\ L^{-1}$	12,420	74,712	2,269	5,271	Log(x)	0.36	1.12	15.9**
Sodium	Na	μ eq L^{-1}	50,065	234,400	7,272	23,881	Log(x)	0.34	1.04	15.0**
% Calcium	%Ca	% cations	4.2	14.8	0.3	2.6	None	0.19	0.49	8.5**
% Potassium	%K	% cations	3.0	5.5	0.8	3.2	None	0.08	0.18	3.5
% Magnesium	%Mg	% cations	18.5	31.6	2.7	18.8	None	0.10	0.22	4.6
% Sodium	%Na	% cations	74.2	94.8	58.3	75.9	None	0.11	0.23	4.6
Cation ratio	Cation-R	(Na + K): (Mg + Ca)	5.01	32.76	1.67	3.89	Log(x)	0.15	0.33	6.7*
Max lake depth	Depth	m	1.0	2.5	0.2	1.0	Square root	0.12	0.26	5.3
Lake area	Area	ha	3.4	10.8	0.1	1.8	Log(x + 1)	0.13	0.29	5.9*

The significance of the percentage of variance explained, based on 999 unrestricted Monte Carlo permutations, is indicated by ** $p < 0.01$ and * $p < 0.1$

Relationships among the environmental variables were explored using principal component analysis (PCA), first on the full dataset (42 lakes), then on the subset of lakes with preserved diatoms (26 lakes). Detrended correspondence analysis (DCA) was used to evaluate patterns of diatom assemblage variation among the lakes and to reveal whether linear or unimodal models were more appropriate for the multivariate analyses. DCA with species data as untransformed percentages were compared with square-root and $\log_{10}$ $(x + 1)$-transformed percentages to assess the robustness of the observed patterns (Ryves et al. 2002).

The relationships between diatoms and environmental data were explored using canonical correspondence analysis (CCA). Transfer functions are more robust for environmental variables that explain relatively large parts of the total variation in the diatom data, independent of any additional variables. Thus, it is important to examine the relative explanatory strength and independence of the variables. In a first series of constrained CCAs, each environmental variable was treated singly. The eigenvalue of CCA axis 1 represents the "marginal" effect and indicates the explanatory power of each variable considered in isolation (Schönfelder et al. 2002). This was done to separate and quantify the effects of each measured environmental variable on the diatom data. The variables that did not explain a significant proportion of the variation in the diatom assemblages were excluded from the following analyses. Then, in a second series of CCAs, forward selection was combined with testing of the significance of each variable using unrestricted Monte Carlo permutation tests and the Bonferroni test (Reed 1998). This was used to identify the minimal number of independent and significant explanatory variables. Finally, in a third series of constrained and partial CCAs, the selected environmental variables were treated singly after the statistical effects of the remaining selected variables were partialed out, treating these variables as co-variables. The proportion of the variance explained by the selected variable, only after fitting co-variables, is called the "partial" or "unique" effect (Schönfelder et al. 2002). The statistical significance of the marginal and unique effects of the variables was tested by 999 Monte Carlo unrestricted permutations. For all constrained and partial CCAs, the amounts of variation explained in each case were transformed to percentages of the total variance by dividing the sum of canonical eigenvalues by the total inertia (Gasse et al. 1995). As for the DCA, the effect of transformation of the diatom percentage data [untransformed, square-root, log (x + 1)] was also examined. All ordination analyses were carried out using CANOCO version 4.5 (ter Braak and Šmilauer 2002).

Additionally, the form of the response of individual species to the main environmental gradient (as identified by CCA), was tested using general additive modeling (GAM). This was done to determine whether the population maximum of a species was situated in the subsaline, hyposaline or mesosaline ranges, and to check how plausible the optima derived by weighted averaging (WA) were. Following Muylaert et al. (2009), only taxa that occurred in >3 samples were tested. Stepwise selection using the Akaike information criterion was used to control the complexity of the GAM model and the maximum number of degrees of freedom for the smoother term was set to two. In addition, we specified the Poisson distribution, with an implied log link function (Lepš and Šmilauer 2003). GAM regressions were carried out using the CanoDraw module of CANOCO (ter Braak and Šmilauer 2002).

To compare the species richness of the surface sediment samples, the counts were standardized using rarefaction analysis. This statistical technique permits an estimation of species richness for samples of different sizes when scaled down to a common size by considering the relative frequencies of individuals (Birks and Line 1992). The diversity measure derived from rarefaction analysis is called the expected species richness, E (Sn), which is the simplest, most useful and most interpretable compositional parameter available for research on sediment sequences. Rarefaction analysis was performed using the program PAST (Hammer et al. 2001).

Transfer functions

Detrended CCA (DCCA), constrained only to the variables of interest, one at a time, was used to further assess the importance of these variables for the diatom assemblages and check which methods, linear or unimodal, were most suitable for building the transfer functions. The length of these environmental gradients, the ratio of the eigenvalue of constrained axis-1 to the eigenvalue of unconstrained axis-2 (λ_1/λ_2), and the correlations between the measured variables and the sample scores on DCCA axis-1 were all examined (Ryves et al. 2002).

As the length of the gradients was long, the unimodal methods of WA and weighted-averaging partial least squares (WA-PLS) were used to develop the transfer-function models (ter Braak and Juggins 1993). Both tolerance down-weighting and simple WA with classical and inverse deshrinking were used. As with previous analyses, the effect of species data transformation was checked. All models were internally validated using bootstrapping methods and performance was evaluated by comparing their coefficient of determination (r^2), their root mean square error of prediction (RMSEP) as estimated by bootstrapping, the RMSEP as a % of the gradient, and the mean and maximum bias. Model building, validation and reconstructions were done using the computer program C2 version 1.6.5 (Juggins 2003–2010).

Application to a sediment core

The transfer function was applied to diatom counts from short sediment sequences from Lakes Zhunaogeqi and Shaobai Jilin, two subsaline lakes with relatively good diatom preservation. For Lake Shaobai Jilin, the sediment core (SHAO07, 33 cm long) was taken with an Uwitec® gravity corer and was sectioned at 1-cm intervals in the field. For Lake Zhunaoeqi, the diatom sequence was built by combining samples from two sediment cores taken from the deepest zone of the lake. The first core (ZHUN08, 19 cm long) was taken in the same way as SHAO07. As this core was too short to record the AD 1963 peak of ^{137}Cs, another, longer core (97 cm) was retrieved with the help of a piston core hammered through the sandy sediment (ZHUN09). This second core was brought back to the Chinese Academy of Sciences in Beijing for extrusion and sampling. The two cores were correlated using the observed changes in the diatom profiles, despite the second core being compressed. ZHUN08 and ZHUN09 were also sectioned at 1-cm intervals.

Dating of the sequences was accomplished by measuring the activity of the radionuclides ^{137}Cs, ^{210}Pb and ^{226}Ra on freeze-dried sediment samples using gamma spectrometry, with a low-background well-type germanium detector (EGPC 100P-15R). Samples were stored in polyethylene tubes for 3 weeks in a sealed container to allow for radioactive equilibration. The samples were then counted for 48 h. Total ^{210}Pb was determined by gamma spectrometry via its energy at 46.5 keV. The short-lived ^{226}Ra daughter nuclides ^{214}Pb and ^{214}Bi were measured to determine supported ^{210}Pb for the calculation of unsupported ^{210}Pb. ^{137}Cs was measured by its emission at 662 keV. Radiometric dates were calculated from the unsupported ^{210}Pb distribution using the constant rate of supply (CRS) model (Appleby 2001) and checked with the ^{137}Cs record.

The diatom profiles were split into diatom assemblage zones (DAZ). These DAZ, based on relative percentages, were delimited using the optimal partitioning procedure of Birks and Gordon (1985). The statistical significance of the zones was evaluated using the broken-stick approach (Bennett 1996). The unpublished programmes ZONE version 1.2 (Lotter and Juggins 1994) and BSTICK version 1.0 (Bennett 1996) were used to generate the zonation.

Weighted analogue matching (WMAT) was used to identify fossil diatom assemblages with good modern analogues to modern assemblages in the calibration dataset. A dissimilarity index based on χ^2 distance was used to compare each fossil sample with all calibration samples. Fossil samples with a minimum dissimilarity lower than the 5th percentile of the dissimilarities for the modern samples were considered "good" analogues (Reavie et al. 2006). These analyses were performed using C2 version 1.6.5 (Juggins 2003–2010).

Remote sensing

Because changes in the depth and extent of Lakes Zhunaogeqi and Shaobai Jilin can impact the composition of their diatom assemblages we investigated the changes in these two lakes using a combination of Google Earth imagery and Landsat and MODIS satellite data. Google Earth was used to outline the current lake boundaries and served as a template to evaluate variation in lake size using Landsat and MODIS. Whereas the Landsat data are higher-resolution ($\sim$15 and 30 m), with a nominal repeat time of every 16 days, only a relatively small percentage of images are cloud-free. Even with this constraint, there were enough cloud-free images (47) from various times of the year between 1990 and 2012 to allow interpretation of lake shore boundaries, water depth and vegetation cover, using bands 8 (15 m panchromatic), 7 (infrared) and 3 and 4 (red and near IR for estimation of the normalized difference vegetation index, NDVI).

MODIS data are at a coarser spatial resolution (250-, 500- and 1,000-m products). However, they are available on a daily basis from 2000 to present with 8- and 16-day products available for download (Oak Ridge 2011). In this analysis, we employed the MOD09 and MOD13 products for analysis of lake extent and NDVI, respectively, using methods outlined in Scuderi et al. (2010). This allowed us to evaluate potential lake extent change on a finer temporal scale, without major data gaps as a consequence of cloud cover.

Results

Environmental data and water chemistry

For the 42 lakes sampled, lake depth and area ranged from 0.1 to 10.7 m and 0.1 to 128 ha, respectively

(Table 1). A large majority of lakes (74 %), however, were shallow (<2 m) and small (<10 ha). The lake water salinity ranged from 1.1 to 237 g L^{-1} and EC ranged from 1.4 to 495 mS cm^{-1}. According to the water salinity classification of Hammer et al. (1983), the training set includes 16 hypersaline lakes (>50 g L^{-1}), which are of two types. Ten of these lakes belong to the group of large and deep lakes that cluster in the northern part of the study area (Fig. 1) and the six others are *salinas*, which are very shallow ponds where a salt crust has formed. The remaining sites include three mesosaline (20–50 g L^{-1}), eight hyposaline (3–20 g L^{-1}) and 15 subsaline lakes (0.5–3 g L^{-1}). No lakes fall within the strict definition of fresh waters (<0.5 g L^{-1}).

The large majority of the lakes are chloride-dominated with either sulphates or carbonates as sub-dominant anions. Only five lakes are carbonate-dominated. All lakes have sodium as the dominant cation (58–97 % of the cations, expressed as mEq L^{-1}), although magnesium is abundant (>20 %) in 11 lakes in the hyposaline and subsaline ranges. Percentages of calcium and potassium never exceed 12 % of the cations.

TP values were extremely variable, with a range of 0–436 μg L^{-1}. All the hypersaline lakes are eutrophic or hypereutrophic in terms of their TP concentrations. The three mesosaline lakes are mesotrophic, whereas the hyposaline and subsaline lakes span the whole range of trophic status from oligotrophic to hypereutrophic (Table 1). TN values ranged from 0.4 to 14.9 mg L^{-1}. The deep hypersaline lakes have low TN values, whereas high TN values characterized the *salinas*. For the lakes classified as subsaline to mesosaline, TN is correlated with salinity ($r = 0.89$). DOC values span a wide range, 2.5–1,510 g L^{-1}, and are generally very high in hypersaline lakes, although the lowest value in the training set was found in a *salina*. When only the subsaline to mesosaline lakes are considered, DOC as for TN, is also correlated with salinity ($r = 0.91$). Si concentrations were very variable (0–10.8 g L^{-1}) and often below detection limits in hypersaline lakes.

Exploratory analysis of the training set

Diatoms were only present in 26 of the 42 lakes sampled. The 16 lakes without diatoms were the most saline in the training set, with values for EC >50,000 μS cm^{-1}, salinity >80 g L^{-1} and pH >10. These 16 lakes were only considered in the exploratory PCA of the environmental variables, but not included in further analyses. In this PCA, the first axis (49.6 %) is highly correlated with salinity, EC and all major ionic concentrations, and separates the hypersaline lakes (>50 g L^{-1}) from the fresher lakes (Electronic Supplementary Material [ESM] Fig. 1a). In a second PCA that includes only the 26 lakes with diatoms present in their surface sediment (ESM Fig. 1b), and therefore excludes the hypersaline lakes, axis 1 (38.9 %) also reflects the major gradient of salinity and separated the mesosaline and hyposaline lakes from the subsaline lakes. None of the 26 lakes was identified as a clear outlier.

A total of 130 diatom taxa were identified in the 26 surface-sediment samples included in the final dataset. After transformation of the counts to relative abundances (%), taxa that could not be resolved to the lowest taxonomic designation possible (species or variety) were excluded from further analysis, which left 128 taxa. Full scientific names of diatom species are given in ESM Appendix 1. The most abundant diatoms in the training set are all littoral species such as *Nitzschia prolongata, Craticula elkab, Staurosira* sp. *1, Navicymbula pusilla* var. *lata* and var. *pusilla, Nitzschia denticula, Nitzschia elegantula, Encyonopsis eifelana* and *Halamphora subcapitata*. There were very few planktonic species and none were abundant, which is likely related to all the lakes of the reduced dataset being small and shallow. There is a distinct turnover of species along the EC gradient (Fig. 2). The expected species richness, E(Sn), calculated by scaling down to the lowest number of valves counted ($n = 254$, Haisen Jilin), ranges from 6.2 (Sayinwusu Xi Hu) to 44.7 (Lake Zhunaogeqi). There is a clear trend of decreasing species diversity with increasing EC (Fig. 2).

Among the 26 surface-sediment samples with diatoms, diatom preservation was very variable, with the F-index ranging from 0.13 (Haisen Jilin) to 0.80 (Baoritelegai Xi Hu) (Fig. 2). There was no statistically significant relationship between diatom preservation and the EC gradient or with most other environmental variables. The F-index was only correlated with lake area ($r = 0.49$, $\alpha = 0.02$). There was also a weak, positive correlation with diatom concentration ($r = 0.47$, $\alpha = 0.02$).

DCA with the diatom species data untransformed, square-root and log (x + 1) transformed gave gradient

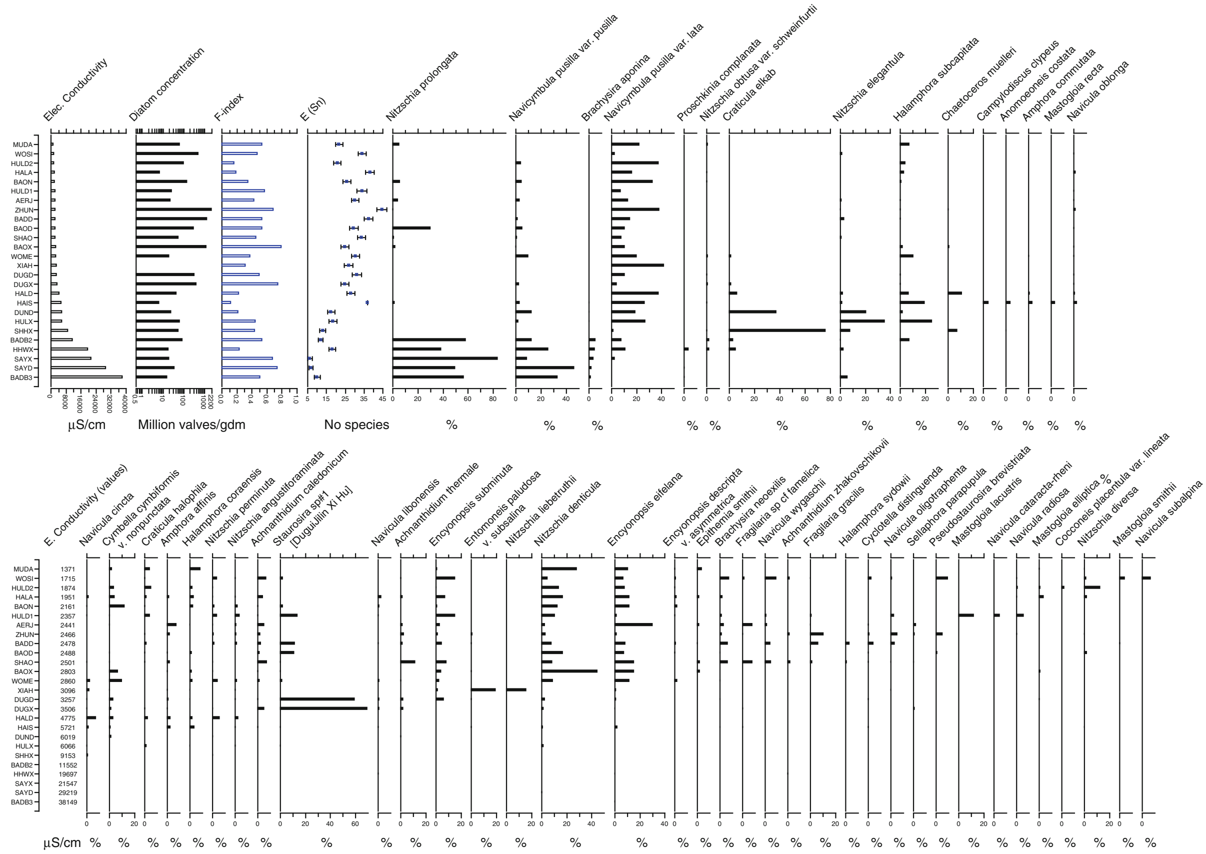

Fig. 2 Distribution of the main species in the 26-lake Badain Jaran surface-sediment training set. All species occurring at 2 % or more in any sample are *plotted* against sites ordered by increasing conductivity from *top* to *bottom*. On the *left-hand side*, the diatom concentration (on a log *scale*), the dissolution index (F) and the expected species richness E(Sn) and its standard error, calculated by rarefaction analysis, are *plotted* for each sample

lengths of 4.29, 3.19 and 3.26 SD units, respectively. These large gradient lengths suggested that most taxa responded non-linearly along the underlying gradients and that unimodal methods were most appropriate to explore the relationship between diatoms and the environmental variables. All 26 diatom-bearing samples were retained for further analyses because no outliers were detected through the DCA of the species data or the PCA of the environmental data.

Canonical correspondence analysis (CCA)

Exploratory CCAs showed that among the 26 environmental variables measured, only a subset accounted for significant portions of the total variance in diatom composition. The variables with the highest percentages of explained marginal variance were EC, Cl, salinity and SO_4 (Table 2). These four variables were highly correlated to each other ($r > 0.95$) and can be considered as different expressions of the same environmental gradient. Marginal explained variance was highest with square-root transformed species data, compared with untransformed and log (% + 1)-transformed data. Only three variables were forward selected in CCA: EC, TP and Area. Partial CCAs indicate that EC has the highest unique effect in terms of partial explained variance and λ_1/λ_2. This reduced set of three variables captured 31.6 % of the total variance in diatom distribution. Axis 1 (explaining 18.3 %) was highly correlated with EC, while axis 2 (8.5 %) was correlated with TP and Area. CCA axis 1 separates meso- and hypo-saline lakes situated on the positive side from the subsaline lakes situated on the negative side. Within both groups, a distinction can be made between the smallest and more eutrophic (high-TP) lakes, situated on the positive side of CCA axis 2

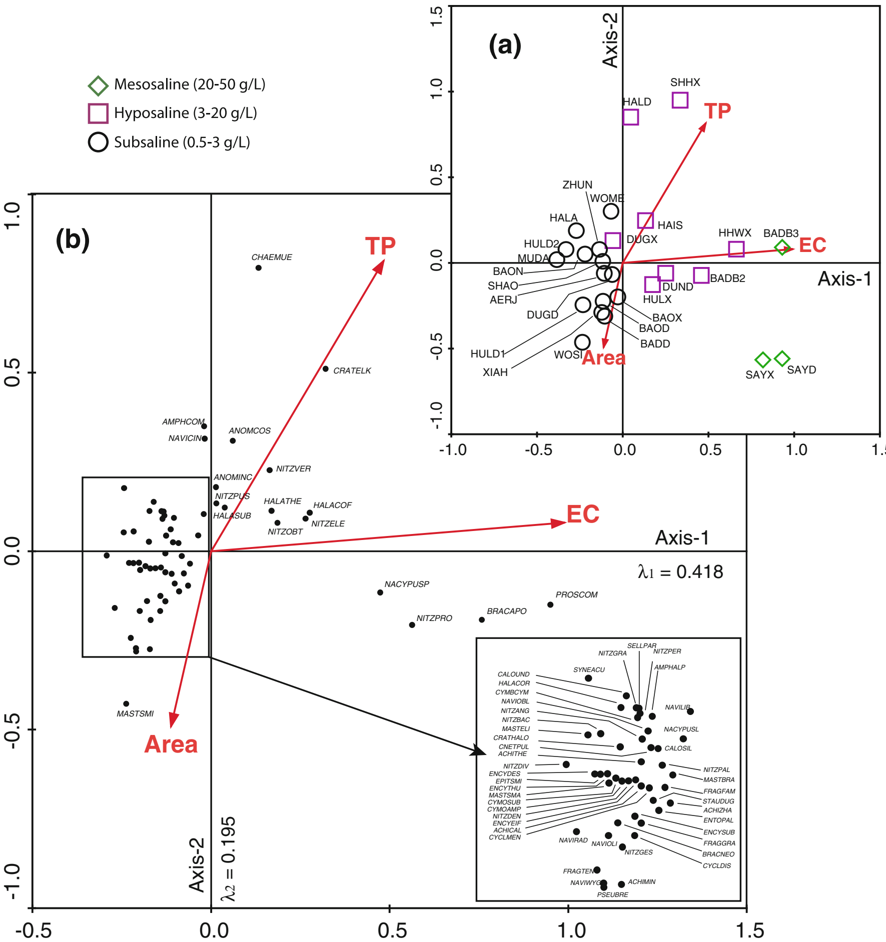

Fig. 3 CCA ordination biplot for the first two *axes*, showing the dominant diatoms (**a**) and the 26 lakes of the Badain Jaran training set (**b**). Only the three environmental variables retained by forward selection (EC, TP, Area) are shown. For this analysis, diatom percentages were square-root transformed. Species codes are given in ESM Appendix 1

and the largest, low-TP lakes situated on the negative side (Fig. 3a). The mesosaline lakes (SAYD, SAYX and BADB3) are characterized by *N. prolongata*, *N pusilla* var. *pusilla* and *Brachysira aponina*. Small and eutrophic hyposaline lakes are mainly characterized by *Chaetoceros muelleri, C. elkab, N. elegantula* and *H. subcapitata*. The subsaline lakes, which are relatively large and mostly oligotrophic, have more diverse assemblages and the main species are *N. pusilla* var. *lata*, *N. denticula*, *Cymbella cymbiformis* var. *nonpunctata*, *E. eifelana*, *Encyonopsis subminuta*, *Achnanthidium caledonicum* and *Brachysira neoexilis* (Fig. 3b).

Diatom response models

Very similar results were obtained for EC and salinity, and only the results for the EC gradient are given here (Fig. 4). Eighty-three species occurred in at least three lakes and were subjected to GAM modeling. Among these, only a minority (10 taxa, 12 %) appeared indifferent in their response to the EC gradient, whereas the large majority (73 taxa, 88 %) shows a significant response. Of these taxa, 53 (63.9 %) had their population maximum in the subsaline range (0.5–3 g L^{-1}; 745–4,480 μS cm^{-1}), 16 (19.3 %) in the hyposaline range (3–20 g L^{-1}; 4,480–29,850 μS cm^{-1}) and 4 (4.8 %) in the mesosaline range (20–50 g L^{-1}; 29,850–74,630 μS cm^{-1}).

EC transfer function

Results of DCCA, performed on un-transformed and transformed diatom data, confirmed that EC was very important in explaining the distribution of diatoms in the assemblages. It has a long gradient length, high λ_1/λ_2 and high correlation between the sample scores on DCCA axis-1 and the observed values for EC (ESM

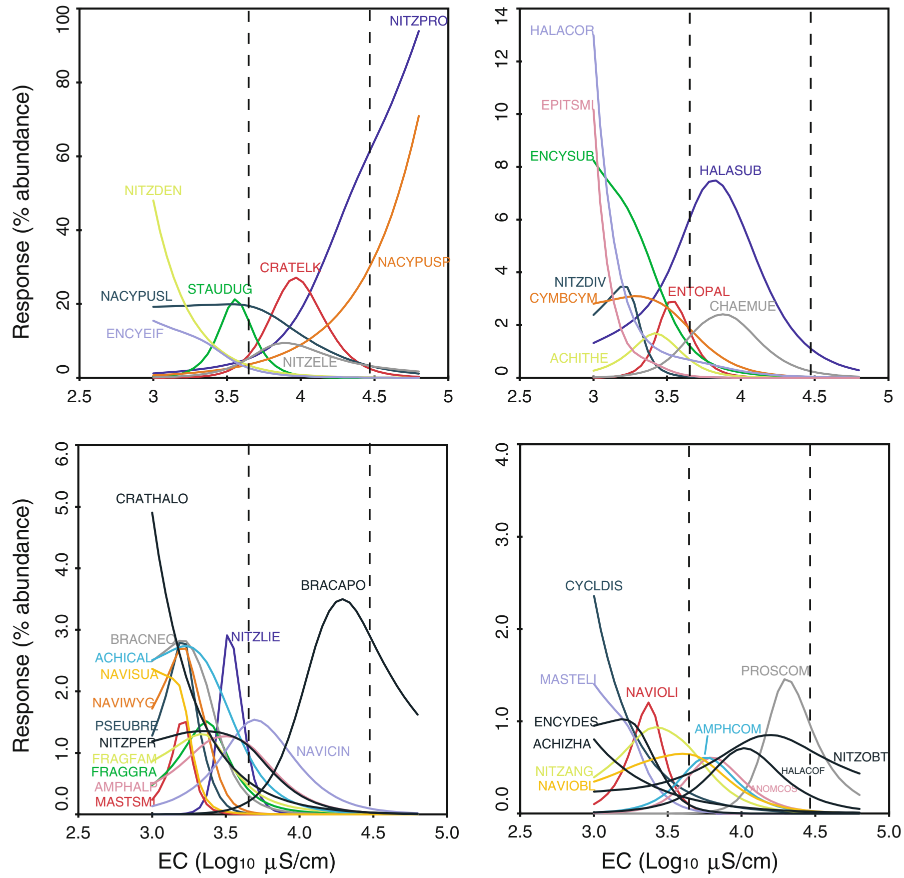

Fig. 4 GAM models of species responses along the EC gradient. Only the responses of the species that contributed to at least 2 % of total abundance in one sample are shown. The vertical dashed lines indicate the limits between the subsaline (4,480 $\approx$ 2.87 $\log_{10}$ µS cm^{-1}), hyposaline (21,850 $\approx$ 4.47 $\log_{10}$ µS cm^{-1}) and mesosaline ranges, respectively. See ESM Appendix 1 for species codes

Table 2). Long gradient lengths also implied that unimodal methods (WA and WA-PLS) were most appropriate. There was little to choose statistically between the various appropriate models (ESM Table 3). The best performing model that combined high bootstrapped r^2 (0.91), low average and maximum bootstrapped bias and low RMSEP (0.136 $\log_{10}$ µS cm^{-1}) was the WA-PLS component 2 model, based on square-root transformed % data (ESM Fig. 2). Gasse et al. (1995) suggested that samples that have a residual >1 quarter of the total range of the variable can be considered outliers. With such a criterion, no sample could be considered an outlier and only one site has high residuals (BADB3), with a residual equivalent to 24.3 % of the EC range.

Dating of Lake Zhunaogeqi sediment cores

For compressed core ZHUN09, the unsupported/supported ^{210}Pb boundary occurred at ~15.5 cm core depth. Unsupported ^{210}Pb activity in this core declined irregularly with depth. The ^{137}Cs activity versus depth profile had a well-resolved peak at ~9.5 cm, indicating the AD 1963 fallout maximum from the atmospheric testing of nuclear weapons (Fig. 5). Comparison of the diatom profiles from ZHUN08 and ZHUN09 suggests that the uppermost sediment layer of ZHUN09 was not retrieved (Fig. 5). Therefore, the ^{210}Pb chronology was calculated based on the assumption that the uppermost 0–1 cm of sediment was missing, and that the core surface was 2005. The simple CRS dating model placed the AD 1963 peak slightly below 9.5 cm. The final chronology was calculated using the CRS model constrained to the AD 1963 depth at ~9.5 cm. ^{210}Pb-based sedimentation rates increase gradually from ~0.05 g cm^{-2} year^{-1} in the AD 1850s to 0.13 g cm^{-2} year^{-1} in the AD 1970s, followed by distinctly increased rates, with a mean of 0.35 g cm^{-2} year^{-1}, in the last 20 years (Fig. 5). Sediment accumulation rate in the upper part

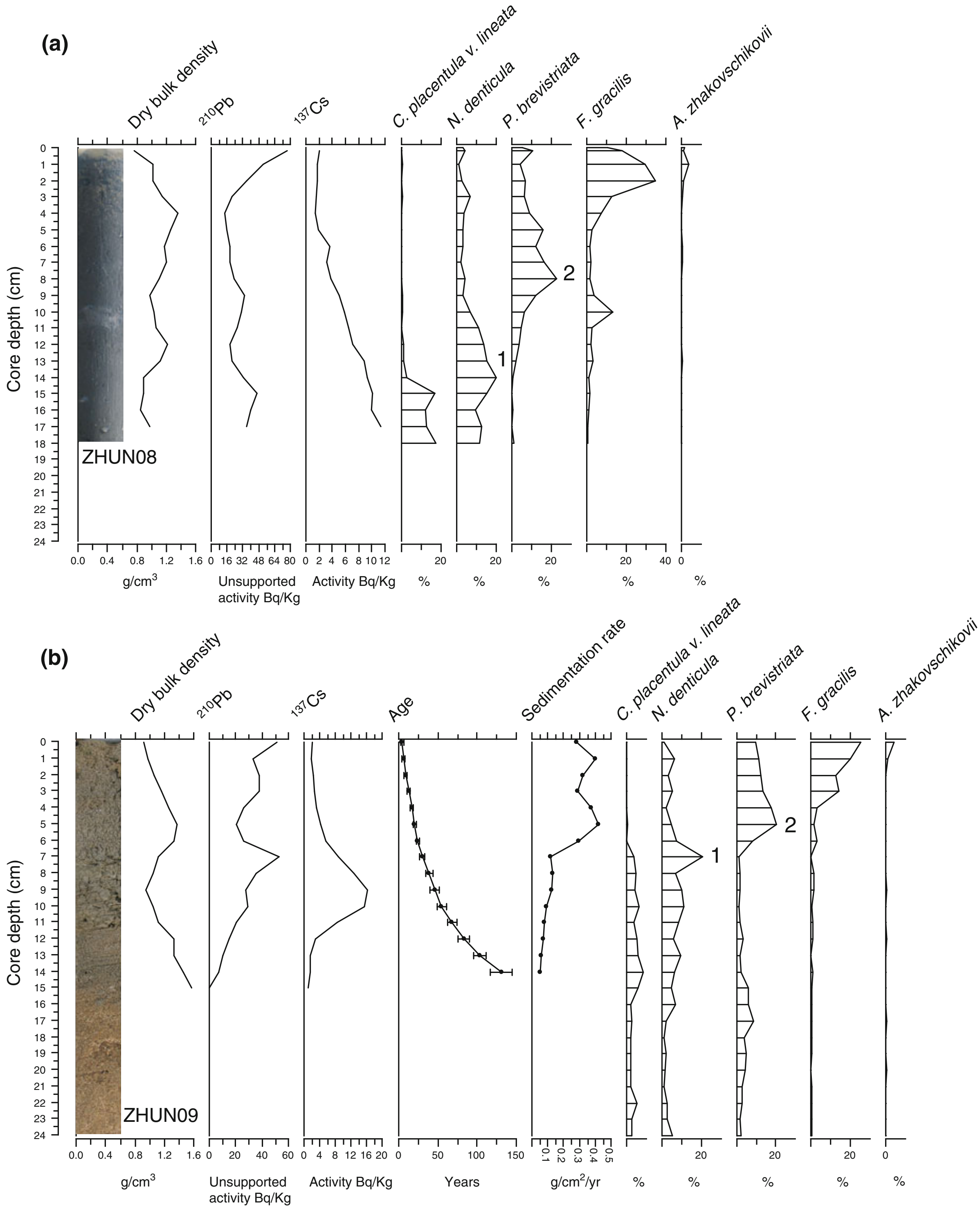

Fig. 5 Radiometric data for **a** core ZHUN08 and **b** core ZHUN09, showing the ^{210}Pb dates derived from the CRS model (*solid lines*) and sedimentation rates (*dashed lines*). In the model for ZHUN09, we assumed that the core *top* was missing and that the sediment surface was 2005. Correlations between cores ZHUN-08 and -09 are based on diatom peaks (1 and 2) and ages for each sample of ZHUN09 were interpolated using a power function

of the core was not constant so it was not appropriate to extrapolate the ^{210}Pb chronology into the past using the average sediment accumulation rate (Appleby 2000). The lowest depth with unsupported ^{210}Pb was 15 cm and dated at AD 1850. Below this core depth, the sediment could not be dated and only the upper part of the core is considered in the discussion.

In core ZHUN08, ^{137}Cs activity increases with depth, indicating that all the sediment (0–18 cm) was deposited after AD 1963. The supported ^{210}Pb depth was not reached. Dating of core ZHUN08 was achieved using the approach described by Campbell (1996), which consists in using a power function (AGE = a + b × DEPTH^{c}) to interpolate dates by correlation of key horizons with a master core that is ^{210}Pb-dated (i.e. ZHUN09). Key horizons used to correlate ZHUN08 with ZHUN09 were peaks in *N. denticula* and *P. brevistriata* (Fig. 5). As shown by Tibby (2001), diatoms can be used for core correlation because their sensitivity to environmental change often results in new assemblages. The power function was calculated by hand, taking age 0 at depth 0 as parameter a, the age 19 at 8.5 cm depth as the value for parameter b (with DEPTH measured in units of 8.5 cm), and solving the equation for the parameter c, where age is 29 and depth is 14.5. Thus, the equation of the power function used for dating ZHUN08 was: AGE = 0 + 19 × [DEPTH/8.5]$^{0.792}$. Finally, a composite profile for Lake Zhunaogeqi (Fig. 6) was constructed by adding a section of core ZHUN09 (before AD 1963, 16 samples, from 9 to 25 cm core depth) to core ZHUN08 (AD 2008–1972, 20 samples). Diatoms were not preserved below 25 cm core depth in ZHUN09.

Dating of Lake Shaobai Jilin sediment core

Unsupported ^{210}Pb activity, which was calculated by subtracting supported ^{210}Pb activity from the total ^{210}Pb activity, declines irregularly with depth. The maximum activity is at 13.5 cm, suggesting an increase in sediment accumulation in recent years. The ^{137}Cs activity displays a well resolved peak at ~25.5 cm and was thus assigned a date of AD 1963 (Fig. 7). Use of the constant initial concentration model (CIC) was precluded because of the non-monotonic variations in unsupported ^{210}Pb activity (Appleby 2001). The final chronology was calculated using the CRS dating model, with reference to the AD 1963 layer identified by the ^{137}Cs record. The inventory of unsupported ^{210}Pb in the core indicates a mean flux to the coring location of ~276 Bq m^{-2} year^{-1}. This is slightly higher than the atmospheric ^{210}Pb deposition flux for the region, suggesting the coring location has been subject to sediment focusing. Sedimentation rates are relatively high in the core. A sediment slump may have occurred in the AD 1950s (Fig. 7).

Lake Zhunaogeqi diatom stratigraphy

Diatom concentration and dissolution show similar trends. Before AD 1950, diatom concentration is low (<30 × 10^{6} valves g^{-1}) and there are very few pristine diatoms (i.e. F-index is close to zero). However, species richness remains relatively high, even in samples with low concentration and high dissolution. Five DAZ were identified using optimal partitioning and the broken-stick model (Fig. 6). ZHUN1 (before AD 1933) is dominated by *N. pusilla* var. *lata,* with *B. neoexilis* and *E. subminuta* also abundant. ZHUN2 (AD 1933–1978) is characterized by a decrease in *N. pusilla* var. *lata* and an increase in *E. eifelana*, *N. denticula*, *Nitzschia diversa.* In the upper part of the zone, *Nitzschia gessneri* and *Cocconeis placentula* var. *lineata* also increase. In ZHUN3 (AD 1978–1986) *E. eifelana* is the most abundant species, with *N. denticula* also abundant. Taxa such as *H. subcapitata, C. cymbiformis* var. *nonpunctata, Craticula halophila, Halamphora coraensis, N. gessneri, Epithemia smithii, Mastogloia elliptica, Navicula radiosa, N. diversa* and *C. placentula* var. *lineata* almost disappear from the assemblages, while the percentages of *Amphora affinis, Achnanthidium thermale, A. caledonicum*, *Fragilaria gracilis, Navicula wygashii, Pseudostaurosira brevistriata* and *Cymbella subhelvetica* increase. ZHUN4 (AD 1986–1997) is marked by a further increase in *N. pusilla* var. *lata* and a peak in *P. brevistriata.* The percentages of *A. thermale, E. subminuta* and *Navicula oligotraphenta* also increase while those of *F. gracilis, N. denticula, N. wygashii* and *C. subhelvetica* decrease. The final zone, ZHUN5 (AD 1997–2008), is characterized by sharp increases of *F. gracilis* and at the very top, *N. pusilla* var. *lata.*

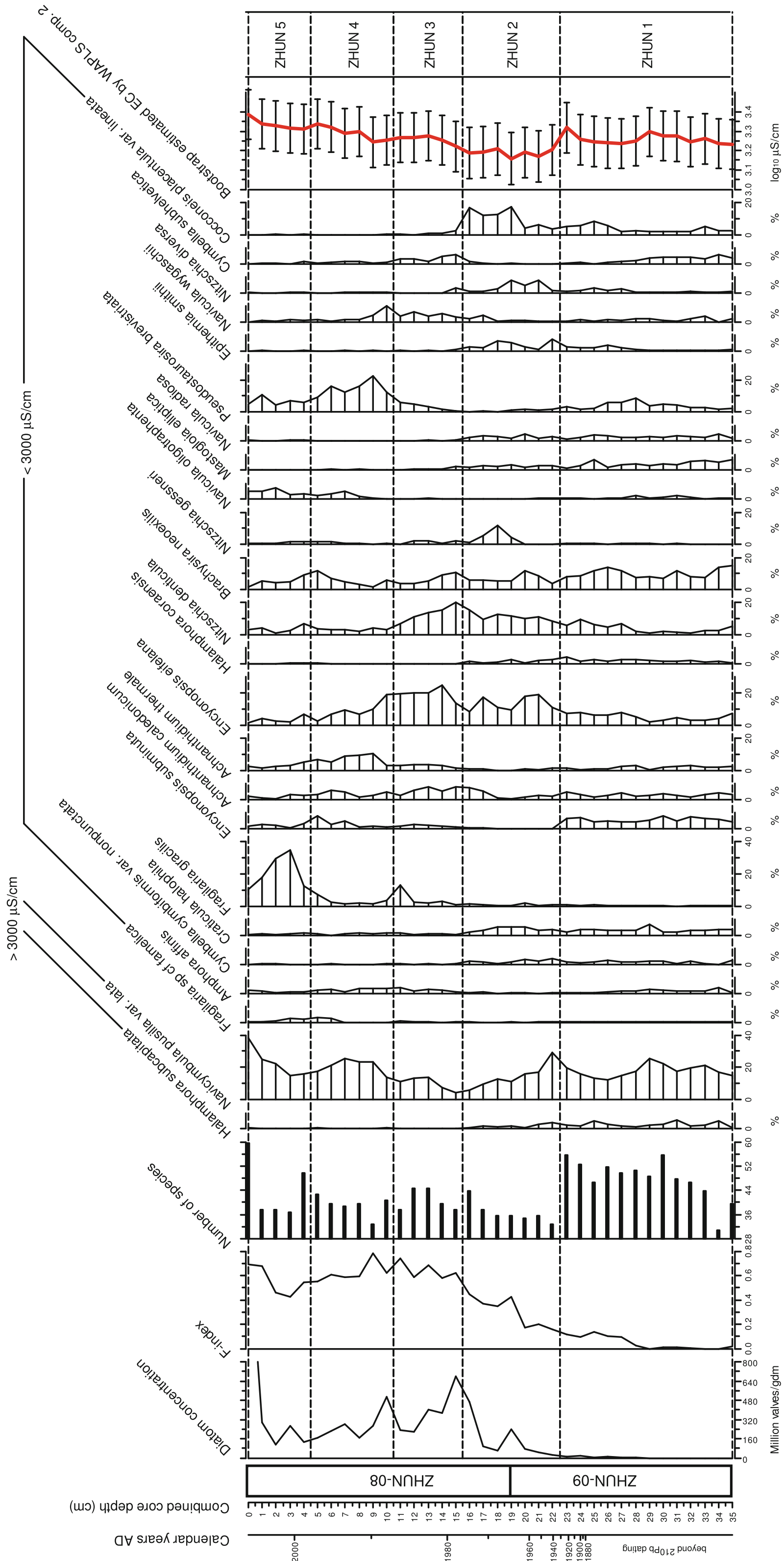

Fig. 6 Summary diatom stratigraphy for the sediment profile from Lake Zhunaogeqi, with cores ZHUN08 and ZHUN09 represented as a single sequence. Only taxa with high relative abundances are shown. Taxa are arranged according to their WA conductivity optima from *left* (*highest*) to *right* (*lowest*). On the *left-handside*, diatom concentration (millions of valves g^{-1} dry matter), the index of valve dissolution (F-index) and the number of species found in each sediment sample are *plotted*. On the *right-handside*, the diatom-inferred EC and the sample-specific error estimates are *plotted*

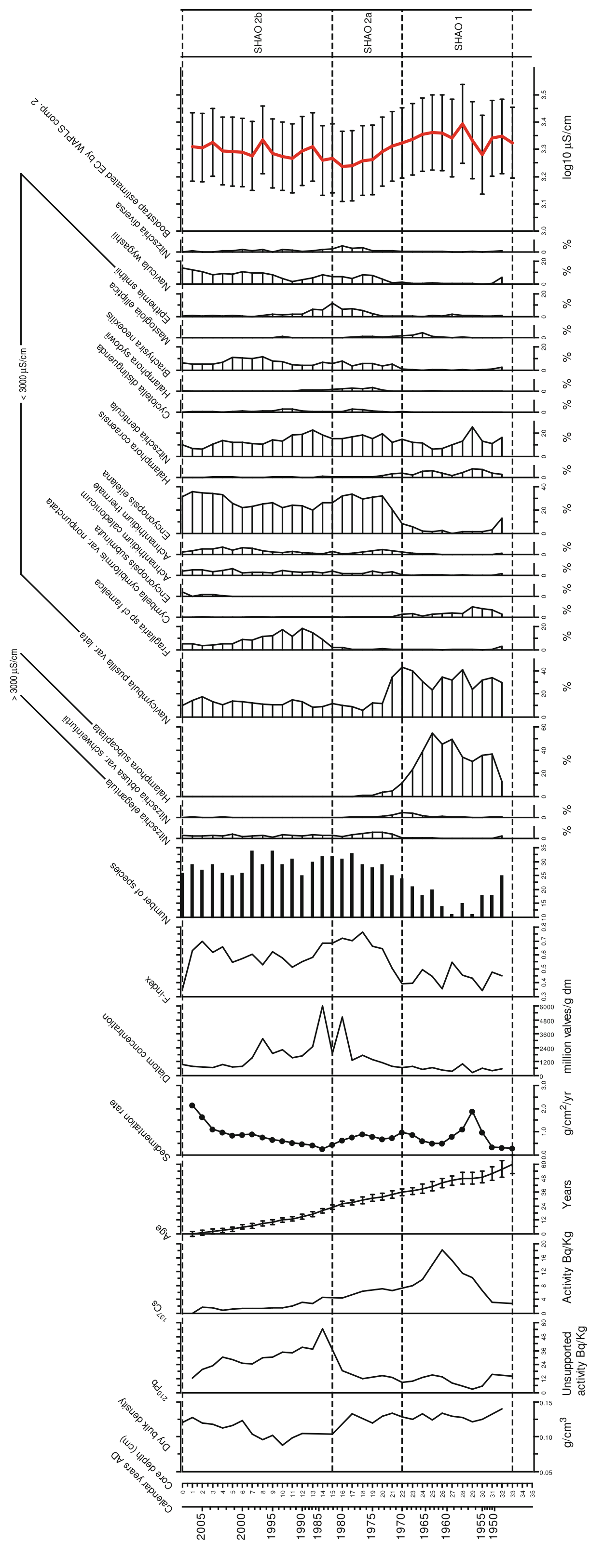

Fig. 7 Summary diagram for the diatom stratigraphy from Lake Shaobai Jilin. Only taxa with high relative abundances are shown. Taxa are arranged according to their WA conductivity optima from *left* (*highest*) to *right* (*lowest*). On the *left-hand side*, diatom concentration (millions of valves g^{-1} dry matter), the index of valve dissolution (F-index) and the number of species found in each sediment sample are *plotted*. On the *right-hand side*, the diatom-inferred EC and the sample-specific error estimates are *plotted*

Lake Shaobai Jilin diatom stratigraphy

Two DAZ were identified. Statistically non-significant sub-zones were also defined for DAZ SHAO2 (Fig. 7). SHAO1 (AD 1947–1970) is characterized by low diatom concentration, relatively high dissolution, low species richness and is dominated by *H. subcapitata* and *N. pusilla* var. *lata.* SHAO2a (AD 1970–1983) is characterized by an increase in diatom concentration, F-index values and species richness, coincident with a sharp decline of *H. subcapitata* and to lesser extent of *N. pusilla* var. *lata* and an increase in *E. eifelana*. SHAO2b (AD 1970–2007) is distinguished from SHAO2a by high percentages of *Fragilaria cf. famelica.*

EC reconstructions

In Lakes Zhunaogeqi and Shaobai Jilin, diatom-inferred (DI) EC varied from 1,445 to 2,440 $\mu S\ cm^{-1}$ (mean = 1,840 $\mu S\ cm^{-1}$, Fig. 6) and from 1,730 to 2,480 $\mu S\ cm^{-1}$ (mean = 2,030 $\mu S\ cm^{-1}$, Fig. 7), respectively. This indicates that the two lakes remained in the subsaline range throughout the sequences. There are similarities and differences in the DI–EC curves for the two lakes. Both had low values in the mid-1970s and early 1980s that are followed by slightly increasing trends until the present. Before the 1970s, the DI–EC curves are different. Lake Zhunaogeqi had high EC during the 1920s and low EC from 1940 to 1970, whereas Lake Shaobai Jilin had high values from 1940 to 1970 (Figs. 6, 7). However, these changes in DI–EC are small in both lakes when we compare them with the sample-specific error estimates that range between 915–1,440 and 1,040–1,690 $\mu S\ cm^{-1}$ for Lakes Zhunaogeqi and Shaobai Jilin, respectively.

Remote sensing

The two remote sensing methods showed that the overall size and depth of the two lakes, as well as that of neighboring lakes, showed no measurable change between 1990 and 2012. The most noticeable variation is an annual increase in the NDVI signal for both the lake pixels and their immediate shoreline pixels. NDVI increases by ~5 %, with a peak in values between late May and early August, synchronous with the maximum temperature signal recorded in the MOD11 land-surface-temperature product. Concomitant with this change in NDVI, there is a slight decrease in reflectance because of an increase in the vegetation canopy of lake-shore pixels and some within-lake pixels with dense stands of aquatic vegetation. This masks the brighter background sand surface. Between September and mid-winter (late January–February), NDVI decreases and reflectance increases.

Discussion

The hydrology of surface waters in the Badain Jaran Desert is imperfectly understood. The large gradient in salinity and chemical composition of the lakes sampled in this study must be the result of several factors. Variation in effective moisture across the desert is, alone, insufficient to explain the variation in salinity, so other factors must be important. In western Nebraska, fresher lakes lie at lower elevation where the main inflow is fresh groundwater, whereas many lakes at higher elevation have limited inputs of groundwater and become more saline by evaporation under an arid climate (Fritz 2008). In the Badain Jaran Desert, however, the position in the watershed does not appear to explain the difference in salinity, as there is no significant relationship between lake surface elevation and EC (r = 0.32 and 0.22 for the 42- and 26-lake datasets, respectively). Yang and Williams (2003) suggested that the more saline northern lakes occupy older basins and that these lakes are more saline simply because they have evolved over a longer period. This, however, does not provide a complete explanation, because differences in salinity amongst the younger lakes in the southeastern part of the desert are also quite large. There, variations in the amount of seepage from the basin, which leads to loss of solutes and hence reduced salinity, may be important (Ma and Edmunds 2006). Therefore, it is likely that climatic, hydrological and geomorphological mechanisms all contribute to the observed patterns of salinity and solute composition in the lakes.

EC gradient and diatom distribution

The EC gradient measured in the Badain Jaran lakes where diatoms were found is not particularly long (1,370–38,150 $\mu S\ cm^{-1}$; 1.1–30.0 $g\ L^{-1}$) compared with other training sets (Table 3). Nevertheless, most of the abundant diatoms in this dataset show a clear response to the EC gradient, as demonstrated by GAM analysis. This is in agreement with other studies in which distinct responses of the diatom flora to even shorter gradients were observed (Ryves et al. 2002). As pointed out by Gell (1997), it is difficult to compare the distributions of taxa (and therefore their estimated optima and tolerance) between training sets from different regions, without carefully harmonizing the diatom taxonomy. Furthermore, optima are influenced by the range and spread of values in the dataset. Nevertheless, the salinity ranking of the Badain Jaran diatoms is coherent with the general ecological information given in diatom floras (Hofmann et al. 2011) and other studies on saline lakes (Cumming et al. 1995; Gasse et al. 1995). The mesosaline lakes of the dataset are characterized by *N. prolongata, N. pusilla* var. *pusilla* and *B. aponina,* whereas species typical of hyposaline lakes include *H. subcapitata, C. elkab, Nitzschia obtusa* var. *schweinfurtii* and *N. elegantula* (Fig. 2). In the subsaline lakes, the diatom flora is remarkable because it is composed of species generally associated with very fresh and even slightly acidic conditions such as *B. neoexilis, N. oligotraphenta, Nitzschia perminuta,* and several species of *Encyonopsis*, together with diatoms commonly found in slightly brackish waters such as *N. pusilla var. lata, N. denticula*, *N. elegantula, Navicula cincta, Navicula libonensis, C. halophila, E. smithii* and several species of *Halamphora* and *Mastogloia.* Species often reported from alkaline springs such as *A. thermale* (Hofmann et al. 2011), *A. zhakovschikovii* (Potapova 2006) and from seepage areas, such as *A. caledonicum* (Wojtal et al. 2011), occur as well. We observed a rapid loss of diversity as salinity increases, in agreement with previous studies on saline lakes (Hammer et al. 1983; Sereda et al. 2011).

The absence of diatoms in hypersaline lakes of the Badain Jaran is, per se, an interesting result. In other arid regions, diatoms have been found in the surface sediments of very salty lakes. For example, diatoms were found in lakes with salinity as high as 270 g L^{-1} in

Fig. 8 Comparison of the diatom-inferred EC reconstructions ▶ with meteorological data from the weather station at Ekenhuduge town in Alashan Youqi county, for the interval AD 1960–2008. **a** Mean annual temperature, **b** mean temperature for the warmest months (April–September), **c** mean temperature for the coldest months (October–March), **d** monthly precipitation, **e** difference between annual precipitation and estimated evaporation from the land surface (=100 mm, Yang et al. 2010), **f** monthly mean wind speed (overlain with the annual mean), **g** and **h** monthly and annual duration of sunshine, **i** back-transformed DI–EC for Lake Zhunaogeqi, **j** back-transformed DI–EC for Lake Shaobai Jilin. In **i** and **j**, the width of the *bars* match the time intervals represented by the core samples and the *plus signs* indicate the *lower* and *upper* sample-specific error

Table 3 Comparison of EC and salinity diatom-transfer function performances from studies around the world

Region/country	References	Nb sites	Gradient	Method	r^2 jack/boot	RMSEP
EC			μS cm^{-1}			Log μS cm^{-1}
Badain Jaran, China	*This study*	*26*	*1370–38,150*	*WA–PLS c2*	*0.91*	*0.14*
N&E Africa	Gasse et al. (1995)	274	40–99,060	WA	0.81	0.39
Spain	Reed (1998)	70	150–338,000	WA	0.57	0.41
Central Mexico	Davies et al. (2002)	53	17–44,100	WA	N/a	0.42
W Greenland	Ryves et al. (2002)	40	24–4,070	WA–PLS c2	0.88	0.22
Tibet/Qinghai, China	Yang XD et al. (2003) and Yang XP et al. (2003)	40	119–116,500	WA–PLS c2	0.92	0.22
	Wang et al. (2011)	87	100–119,400	WA	0.74	0.38
NW Mongolia	Shinneman et al. (2009)	54	41–32,300	WA	0.81	0.39
Turkey	Reed et al. (2012)	91	142–125,000	WA	0.78	0.41
Salinity			g L^{-1}			Log g L^{-1}
Badain Jaran, China	*This study*	*26*	*1.1–30*	*WA*	*0.89*	*0.14*
N Great Plains, USA	Fritz et al. (1993)	66	0.65–270	WA	N/a	0.53
Brit. Columbia, Canada	Wilson et al. (1996)	219	0.04–620	WA	0.87	0.37
W. Victoria, Australia	Gell (1997)	73	0.5–133	WA	0.79	0.29
East Antarctica	Verleyen et al. (2003)	111	0.1–165	WA	0.83	0.31

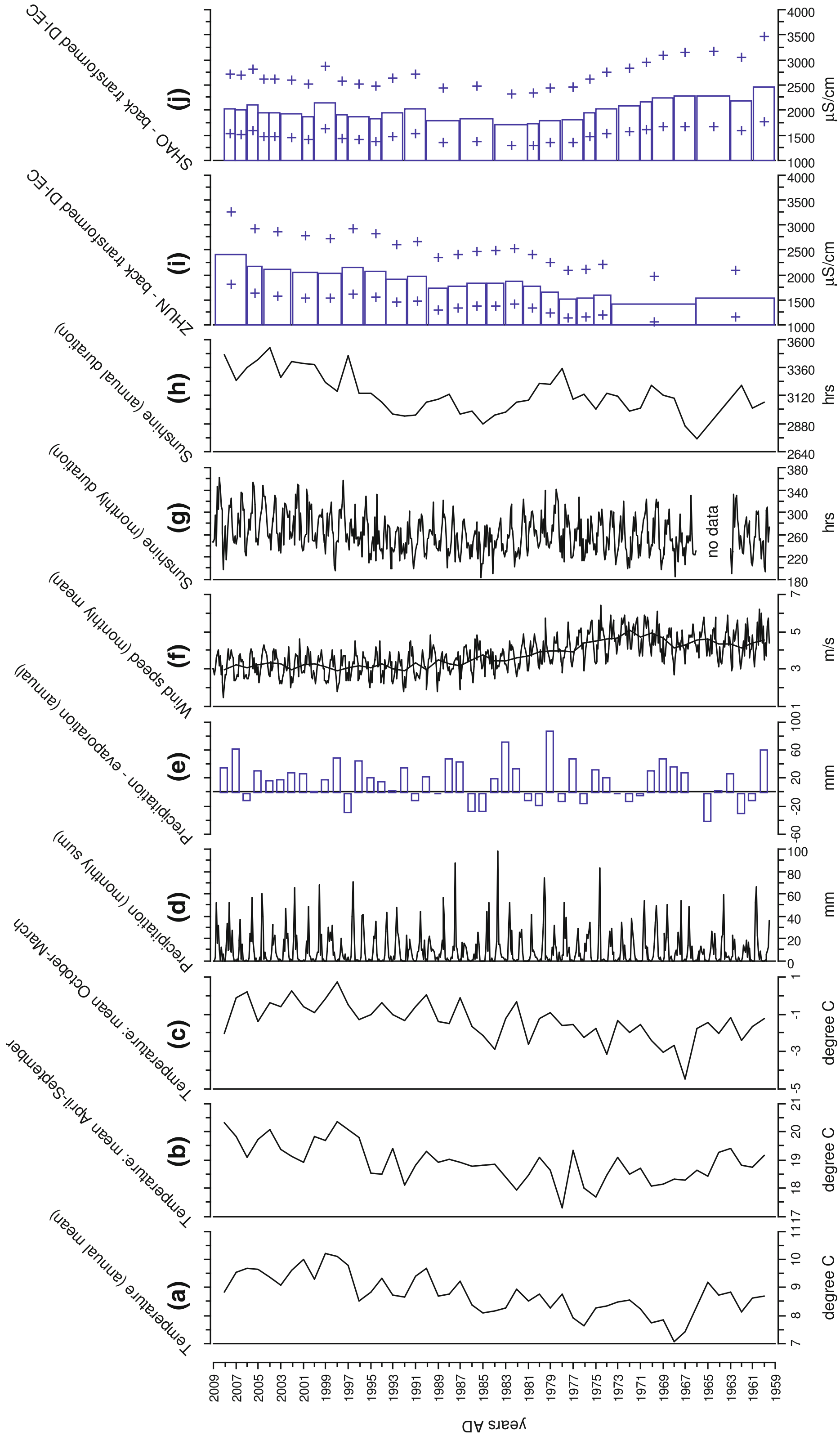
(a) Temperature (annual mean)
(b) Temperature: mean April-September
(c) Temperature: mean October-March
(d) Precipitation (monthly sum)
(e) Precipitation - evaporation (annual)
(f) Wind speed (monthly mean)
(g) Sunshine (monthly duration)
(h) Sunshine (annual duration)
(i) ZHUN - back transformed DI-EC
(j) SHAO - back transformed DI-EC
no data
degree C
mm
m/s
hrs
µS/cm
years AD

the Great Plains, USA (Fritz et al. 1993), 620 g L^{-1} in British Columbia, Canada (Wilson et al. 1996) and 1,020 g L^{-1} in Mexico (Davies et al. 2002). High salinity itself is therefore not sufficient to suppress diatoms completely. In the hypersaline lakes studied here, diatoms were not found in surface sediment samples or in water and epipsammon samples. Thus, we assume that the absence of diatoms was not caused by non-preservation of valves at the sediment–water interface, but more generally by conditions unsuitable for the development of diatoms in these lakes. Several factors may contribute to this situation, including high pH (in the 16 hypersaline lakes of the dataset, mean pH value is 10.2), under-saturation with respect to Si (Barker 1992) and the binding of PO_4 by DOC and salts, making the nutrient unavailable to algae (Sereda et al. 2011). In one lake (Badan Xi Hu) low light conditions, a consequence of high turbidity, may have also played a role in suppressing diatoms. For the *salinas* (BADB1, HHWD, HHWX, SUHA, TONG), periodic desiccation may also prevent diatoms from developing.

To our knowledge, the only published works on the diatom flora of the Badain Jaran lakes are those of Hofmann (1996) and Hahn and Hofmann (1999). These authors analyzed plankton samples from several lakes that span the entire salinity gradient. As in our study, they found *Cymbella pusilla* (=*N. pusilla*) and *Denticula kuetzingii* (=*N. denticula*) among the dominant diatoms in the less saline lakes. However, in total disagreement with our findings, they also reported the presence of planktonic diatoms in two hypersaline lakes, including species not known to be associated with salty waters, such as *Cyclotella comensis, Cyclotella bodanica* var. *affinis, Stephanodiscus neoastraea, Tabellaria flocculosa* and *Asterionella formosa*. Because their samples were collected with a plankton net, we suspect they were contaminated with diatoms from freshwater lakes during previous sampling.

Diatom dissolution

If we exclude hypersaline lakes, diatoms were generally well preserved in the surface sediment samples. In the surface sediments of saline lakes from Greenland and the Northern Great Plains, USA, Ryves et al. (2006) found that dissolution generally increased along the salinity gradient, but this is not the case in our dataset. The relationship between the F-index and lake area in the dataset suggests that diatoms are exposed to more breakage and dissolution in the surface sediment of the smallest (and shallowest) sites, as these are most likely to dry periodically and are more affected by wind-driven turbulence.

In the down-core samples of the Lake Zhunaogeqi sediment core, the F-index shows that diatom dissolution increases steadily to the point where no diatom remains are preserved at 25 cm depth (36 cm if the depth of the combined profile is considered, Fig. 6). Similar results were obtained in cores from all other investigated lakes in the Badain Jaran Desert (Rioual et al. unpublished data). However, relatively fragile diatoms in the Lake Zhunaogeqi core are present and the number of taxa remains fairly high ($n = 31$–60) throughout the profile, which suggests that selective preservation was not so severe that the assemblages contain only the remains of a few, very robust taxa (Ryves et al. 2001).

Palaeosalinity records

Reliability of the DI–EC reconstructions

One way to assess the reliability of a transfer function is to examine the bootstrapped residuals for the surface sediment of the sites to which the transfer function is applied (Ryves et al. 2002). Using this criterion, the WA-PLS component-2 model gave very low residuals for lakes Zhunaogeqi and Shaobai Jilin, with small underestimates of 19 and 123 µS cm^{-1}, respectively. In Lake Zhunaogeqi, 87 out of the 98 species in the core samples are also present in the calibration dataset and the sum of their percentages represents at least 90 % of the total count. For Lake Shaobai Jilin, 60 of 64 "fossil" species are present in the dataset and they represent at least 98 % of the assemblages. However, "fossil" species are often recorded at different relative abundances than observed in the modern calibration set samples and MAT analysis shows that for Lake Zhunaogeqi, only four core samples at the top of the sequence have good modern analogues (within the 5th percentile of dissimilarities). For Lake Shaobai Jilin, 16 out of 33 samples have good modern analogues.

Comparison of the EC reconstructions with meteorological data

Among the various factors that can cause EC to vary in these lakes are climate (i.e. the balance between precipitation and evaporation), the amount of groundwater inflow (itself influenced by climate, but also by geomorphological processes) and changes in the quality of groundwater. It seems reasonable to exclude this last factor and assume that the chemical composition and EC of groundwater has remained constant over the short period investigated here, because the ages of groundwater in the Badain Jaran Desert, which could be estimated by measuring their tritium content, range between 40 and 100 years (Yang and Williams 2003).

We have limited data on the seasonal variations in EC for some of the lakes. Nevertheless, a seasonal pattern can be summarized as follows. During winter, thick ice-cover affects the subsaline lakes (hypersaline lakes do not freeze) and the evaporation from the lake surface is close to zero (Yang et al. 2010). When the ice melts in spring the lakes have low EC values, then throughout the summer and autumn seasons EC increases due to surface-water evaporation. Over a longer time-scale, we cannot verify the EC reconstructions, as we do not have long-term monitoring data for EC or salinity.

To assess the recent variations in climate, we used the meteorological data from the Ekenhuduge weather station, for the period AD 1959–2008 (Fig. 8). The temperature record is representative of the marked recent warming trend in Inner Mongolia (0.4 °C per decade) (Piao et al. 2010). An increase in sunshine duration is also noticeable since AD 1995 (Fig. 8) and there has been a steady decrease in windiness since the early 1970s (Fig. 8). This agrees with the trend observed for the northern Hemisphere over the past few decades (Vautard et al. 2010). A continuous decrease in the amount, frequency and intensity of precipitation has been recorded in the wider region of north-central China (Ma and Fu 2006). However, precipitation data from Ekenhuduge show that in most years since AD 1959, annual precipitation was >100 mm (Fig. 8), which is the value for the mean annual evaporation from land surfaces obtained by Yang et al. (2010). This indicates that in recent years, local rainfall was high enough to contribute to the recharge of groundwater.

The sensitivity of the lakes to variation in climate can be evaluated by comparing the DI reconstructions with the modern instrumental climate data. This is also done to check if the studied lakes behave in a predicable way (Fritz 2008). We checked for correlations between the DI–EC records and the monthly meteorological data. For this purpose, the meteorological data were averaged for the time intervals corresponding to the core samples. The DI–EC record of Lake Shaobai Jilin was not correlated significantly with the meteorological variables, except for a weak positive correlation with the mean monthly wind speed ($r = 0.47$, $\alpha = 0.02$). For Lake Zhunaogeqi, no significant relationship was observed with the precipitation data, which is characterized by large interannual variations, or with the mean monthly temperature. However, there were weak positive correlations with the mean temperature of the warm months (April–September) ($r = 0.44$, $\alpha = 0.05$), the mean temperature of the cold months (October–March) ($r = 0.52$, $\alpha = 0.02$) and the mean of the monthly duration of sunshine ($r = 0.48$, $\alpha = 0.05$). A strong negative correlation was also observed between the DI–EC of Lake Zhunaogeqi and wind speed ($r = -0.85$, $\alpha = 0.001$). This may be a spurious correlation, as higher wind speed would tend to increase, rather than reduce evaporation and EC.

A positive relationship between DI–EC and the recent increase in temperature has been reported from Tibet (Wang et al. 2011). The increasing trend in DI–EC that we observed in Lake Zhunaogeqi from the 1980s appears also to follow the temperature curve, suggesting that enhanced evaporation caused EC to increase (Fig. 8). However, the increase in EC at Lake Zhunaogeqi is very small (within the error range of the reconstruction) and in Lake Shaobai Jilin no such increase was observed. Moreover, remote sensing data indicate that the extent of the lakes and their water depth did not change during the past decade. Therefore, whereas remote sensing data does not provide information on past variations in EC, it confirms that losses due to evaporation were compensated by recharge through groundwater inflow, so that lake levels did not decline, at least over the past decade.

In summary, over the past 50 years the two lakes investigated had different values and trends for EC and appear to have been mainly controlled by hydrogeological rather than climatic factors. Furthermore, remote sensing data indicate that even when lakes appear to respond to climate, this response is mediated by groundwater inflow.

Conclusions

This study shows that a strong relationship exists between the composition of modern diatom assemblages and the major hydrochemical variables in lakes of the Badain Jaran Desert, China. Using multivariate statistical techniques, we demonstrated that EC makes a highly significant and independent contribution to the total variance in the diatom data. A transfer function quantifying these relationships could be developed to reconstruct EC from sedimentary diatom sequences, although the model is based on a relatively low number of lakes. The predictive ability of this model compares well with those developed in other regions around the world. To illustrate the potential of this transfer function, it was applied to two short sediment records spanning at most the last *ca.* 120 years. The DI–EC reconstructions were compared with remote sensing data for the past 10 years and local meteorological data over the past 50 years. This comparison suggests that the response of these lakes to climate is mediated by non-climatic factors that may be non-linear and non-stationary. Regrettably, analysis of a longer record is hampered by diatom dissolution in downcore samples. To pursue this work, we will sample more sites, focusing on the extensive arid area of eastern Inner Mongolia, where there are numerous saline lakes. Eventually we will merge this dataset with the larger ones developed from Qinghai and Tibet (Yang XD et al. 2003; Wang et al. 2011).

Acknowledgments This research was funded by the National Natural Science Foundation of China (Grant Number: 40930105) and the Chinese Academy of Sciences (Grant Number: kzcx2-yw-119). We thank Oliver Heiri, Mark Brenner and two anonymous reviewers for their constructive comments on the manuscript.

References

Appleby PG (2000) Radiometric dating of sediment records in European mountain lakes. J Limnol 59:1–14
Appleby PG (2001) Chronostratigraphic techniques in recent sediments. In: Last WM, Smol JP (eds) Tracking environmental change using lake sediments: basin analysis, coring, and chronological techniques, vol 1. Kluwer, Dordrecht, pp 171–203
Barker PA (1992) Differential diatom dissolution in late Quaternary sediments from Lake Manyara, Tanzania: an experimental approach. J Paleolimnol 7:235–251
Battarbee RW, Kneen MJ (1982) The use of electronically counted microspheres in absolute diatom analysis. Limnol Oceanogr 27:184–188
Bennett KD (1996) Determination of the number of zones in a biostratigraphic sequences. New Phytol 132:155–170
Birks HJB, Gordon AD (1985) Numerical methods in Quaternary pollen analysis. Academic Press, London
Birks HJB, Line JM (1992) The use of rarefaction analysis for estimating palynological richness from Quaternary pollen-analytical data. Holocene 2:1–10
Bronk DA, Lomas MW, Glibert PM, Schukert KJ, Sanderson MP (2000) Total dissolved nitrogen analysis: comparisons between the persulfate, UV and high temperature oxidation methods. Mar Chem 69:163–178
Campbell ID (1996) Power function for interpolating dates in recent sediment. J Paleolimnol 15:107–110
Cumming BF, Wilson SE, Hall RI, Smol JP (1995) Diatoms from British Columbia (Canada) lakes and their relationships to salinity, nutrients and other limnological variables. J. Cramer, Berlin
Davies SJ, Metcalfe SE, Caballero ME, Juggins S (2002) Developing diatom-based transfer functions for Central Mexican lakes. Hydrobiologia 467:199–213
Endoh S, Tsujii I, Kawashima M, Okumura Y (2008) A new method for temperature compensation of electrical conductivity using temperature-fold dependency of fresh water. Limnology 9:159–161
Fritz SC (2008) Deciphering climatic history from lake sediments. J Paleolimnol 39:5–16
Fritz SC, Juggins S, Battarbee RW (1993) Diatom assemblages and ionic characterization of lakes of the Northern Great Plains, North America: a tool for reconstructing past salinity and climate fluctuations. Can J Fish Aquat Sci 50:1844–1856
Gasse F, Juggins S, Ben Khelifa L (1995) Diatom-based transfer functions for inferring past hydrochemical characteristics of African lakes. Palaeogeogr Palaeoclimatol Palaeoecol 117:31–54
Gell PA (1997) The development of a diatom database for inferring lake salinity, Western Victoria, Australia: towards a quantitative approach for reconstructing past climates. Aust J Bot 45:389–423
Gran G (1952) Determination of the equivalence point in potentiometric titrations. Part II. Analyst 77:661–671
Hahn A, Hofmann J (1999) Mikroalgen einer hydrologisch vielfältigen Seengruppe im Megadünengebiet der Badain Jaran Wüste/VR China. Berichte des IGB H7:59–62
Hammer UT, Shamess J, Haynes RC (1983) The distribution and abundance of algae in saline lakes of Saskatchewan, Canada. Hydrobiologia 105:1–26
Hammer Ø, Harper DAT, Ryan PD (2001) PAST: paleontological statistics software package for education and data analysis. Palaeontol Electron 4:1–9
Hofmann J (1996) The lakes in the SE part of Badain Jaran Shamo, their limnology and geochemistry. Geowissenschaften 14:275–278
Hofmann G, Werum M, Lange-Bertalot H (2011) Diatomeen im Süßwasser-Benthos von Mitteleuropa. A.R.G. Gantner Verlag K.G., Ruggell
Jones MN (1984) Nitrate reduction by shaking with cadmium. Water Res 18:643–646
Juggins S (2003–2010) C2 data analysis. Version 1.6.5. University of Newcastle, Newcastle

Krammer K (1997) Die cymbelloiden Diatomeen. Eine Monographie der weltweit bekannten Taxa. Teil 2. *Encyonema* part., *Encyonopsis* and *Cymbellopsis*. J. Cramer, Berlin

Lange-Bertalot H (2001) Navicula sensu stricto. 10 genera separated from Navicula sensu lato. *Frustulia*. A.R.G. Gantner Verlag K.G., Ruggell

Lepš S, Šmilauer P (2003) Multivariate analysis of ecological data using CANOCO. Cambridge University Press, Cambridge

Levkov Z (2009) Amphora sensu lato. A.R.G. Gantner Verlag K.G., Ruggell

Lotter AF, Juggins S (1994) ZONE. Unpublished computer software

Ma J, Edmunds WM (2006) Groundwater and lake evolution in the Badain Jaran Desert ecosystem, Inner Mongolia. Hydrogeol J 14:1231–1243

Ma Z, Fu C (2006) Some evidence of drying trend over northern China from 1951 to 2004. Chin Sci Bull 51:2913–2925

Metzeltin D, Lange-Bertalot H, Soninkhishig N (2009) Diatoms in Mongolia. A.R.G. Gantner Verlag K.G., Ruggell

Muylaert K, Sabbe K, Vyverman W (2009) Changes in phytoplankton diversity and community composition along the salinity gradient of the Schedele estuary (Belgium/The Netherlands). Estuar Coast Shelf Sci 82:335–340

Oak Ridge National Laboratory Distributed Active Archive Center (ORNL DAAC) (2011) MODIS subsetted land products, collection 5. ORNL DAAC, Oak Ridge. Available on-line (http://daac.ornl.gov/MODIS/modis.html). Accessed 06 Jan 2012

Piao S, Ciais P, Huang Y, Shen Z, Peng S, Li J, Zhou L, Liu H, Ma Y, Ding Y, Friedlingstein P, Liu C, Tan K, Yu Y, Zhang T, Fang J (2010) The impacts of climate change on water resources and agriculture in China. Nature 467:43–51

Potapova M (2006) *Achnanthidium zhakovschikovii* sp. nov. (Bacillariophyta) and related species from rivers of Northwestern Russia. Nova Hedwigia 82:399–408

Reavie ED, Neill KE, Little JL, Smol JP (2006) Cultural eutrophication trends in southeastern Ontario lakes: a paleolimnological perspective. Lake Reserv Manag 22:44–58

Reed JM (1998) A diatom–conductivity transfer function for Spanish salt lakes. J Paleolimnol 19:399–416

Reed JM, Mesquita-Joanes F, Griffiths HI (2012) Multi-indicator conductivity transfer functions for Quaternary palaeoclimate reconstruction. J Paleolimnol 47:251–275

Renberg I (1990) A procedure for preparing large sets of diatom slides from sediment cores. J Paleolimnol 4:87–90

Ryves DB, Juggins S, Fritz SC, Battarbee RW (2001) Experimental diatom dissolution and the quantification of microfossil preservation in sediments. Palaeogeogr Palaeoclimatol Palaeoecol 172:99–113

Ryves DB, McGowan S, Anderson NJ (2002) Development and evaluation of a diatom-conductivity model from lakes in West Greenland. Freshw Biol 47:995–1014

Ryves DB, Battarbee RW, Juggins S, Fritz SC, Anderson NJ (2006) Physical and chemical predictors of diatom dissolution in freshwater and saline lake sediments in North America and west Greenland. Limnol Oceanogr 51:1355–1368

Schönfelder I, Gelbrecht J, Schönfelder J, Steinberg CEW (2002) Relationships between littoral diatoms and their chemical environment in northeastern German lakes and rivers. J Phycol 38:66–82

Scuderi LA, Laudadio CK, Fawcett PJ (2010) Remote sensing of Playa lakes in western North America: monitoring lake change resulting from climate variability in semi-arid regions. Quat Res 73:48–58

Sereda J, Bogard M, Hudson J, Helps D, Dessouki T (2011) Climate warming and the onset of salinization: rapid changes in the limnology of two northern plains lakes. Limnologica 41:1–9

Shinneman ALC, Edlund MB, Almendinger JE, Soninkhishig N (2009) Diatoms as indicators of water quality in Western Mongolian lakes: a 54-site calibration set. J Paleolimnol 42:373–389

ter Braak CJF, Juggins S (1993) Weigthed averaging partial least squares regression (WA-PLS): an improved method for reconstructing environmental variables from species assemblages. Hydrobiologia 269(270):485–502

ter Braak CJF, Šmilauer P (2002) CANOCO for Windows version 4.5. Biometris, Wageningen

Tibby J (2001) Diatoms as indicators of sedimentary processes in Burrinjuck reservoir, New South Wales, Australia. Quat Int 83(85):245–256

Vautard R, Cattiaux J, Yiou P, Thépaut J-N, Ciais P (2010) Northern hemisphere atmospheric stilling partly attributed to an increase in surface roughness. Nat Geosci 3:756–761

Verleyen E, Hodgson DA, Vyverman W, Roberts D, McMinn A, Vanhoutte K, Sabbe K (2003) Modelling diatom responses to climate induced fluctuations in the moisture balance in continental Antarctic lakes. J Paleolimnol 30:195–215

Wang R, Yang X, Langdon P, Zhang E (2011) Limnological responses to warming on the Xizang Plateau, Tibet, over the past 200 years. J Paleolimnol 45:257–271

Wetzel RG, Likens GE (2000) Limnological analysis, 3rd edn. Springer, New York

Wilson SE, Cumming BF, Smol JP (1996) Assessing the reliability of salinity inference models from diatom assemblages: an examination of a 219-lake data set from western North America. Can J Fish Aquat Sci 53:1580–1594

Witkowski A, Lange-Bertalot H, Metzeltin D (2000) Diatom flora of marine coasts I. A.R.G. Gantner Verlag K.G., Ruggell

Wojtal AZ, Ector L, Van de Vijver B, Morales EA, Blanco S, Piatek J, Smieja A (2011) The *Achnanthidium minutissimum* complex (Bacillariophyceae) in southern Poland. Algol Stud 136–137:211–238

Yang XD, Kamenik C, Schmidt R, Wang S (2003) Diatom-based conductivity and water-level inference models from eastern Tibetan (Qinghai–Xizang) Plateau lakes. J Paleolimnol 30:1–19

Yang XP (2000) Landscape evolution and precipitation changes in the Badain Jaran Desert during the last 30,000 years. Chin Sci Bull 45:1042–1047

Yang XP, Williams MAF (2003) The ion chemistry of lakes and late Holocene desiccation in the Badain Jaran Desert, Inner Mongolia, China. Catena 51:45–61

Yang XP, Liu TS, Xiao H (2003) Evolution of megadunes and lakes in the Badain Jaran Desert, Inner Mongolia, China during the last 31,000 years. Quat Int 104:99–112

Yang XP, Ma N, Dong J, Zhu B, Xu B, Ma Z, Liu J (2010) Recharge to the inter-dune lakes and Holocene climatic changes in the Badain Jaran Desert, western China. Quat Res 73:10–19